



Lawrence Berkeley Laboratory

UNIVERSITY OF CALIFORNIA

Engineering & Technical Services Division

RECEIVED
LAWRENCE
BERKELEY LABORATORY
JUN 15 1982
LIBRARY AND
DOCUMENTS SECTION

Submitted to Nuclear Instruments and Methods

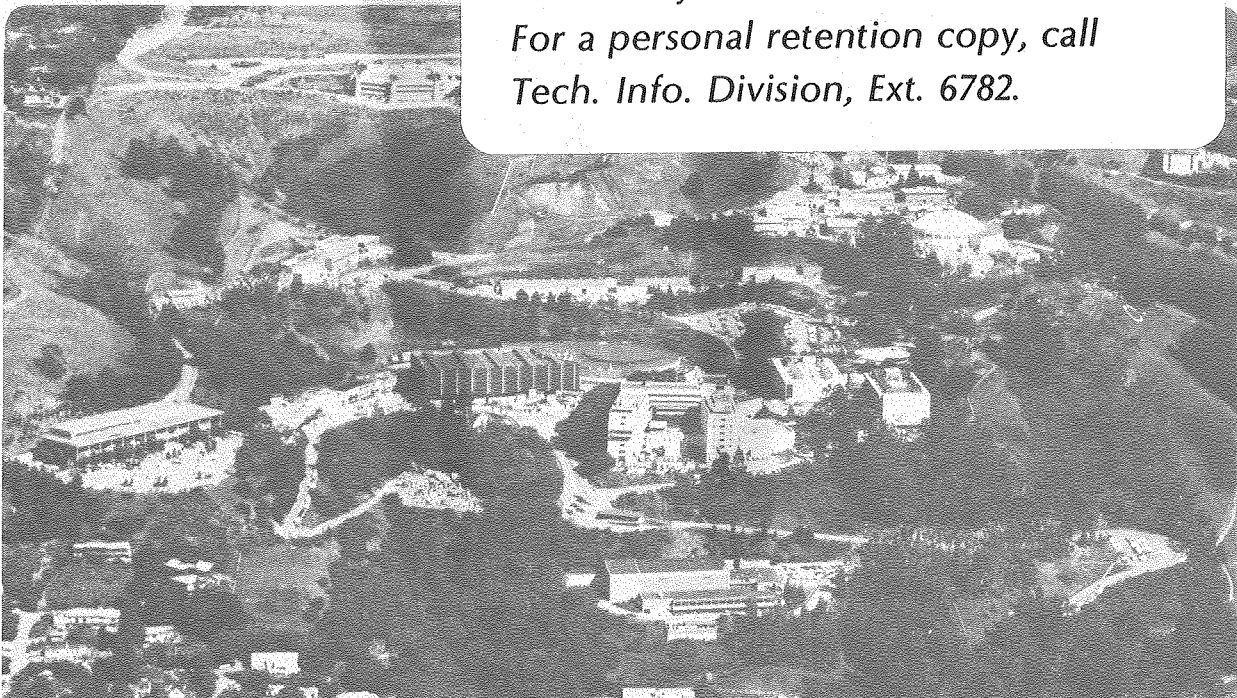
CHARACTERIZATION OF LARGE DIAMETER SILICON BY
LOW-BIAS CHARGE COLLECTION ANALYSIS IN Si(Li)
PIN DIODES

Abraham Fong, Jack T. Walton, Eugene E. Haller,
Heinrich A. Sommer and Jens Guldborg

January 1981

TWO-WEEK LOAN COPY

*This is a Library Circulating Copy
which may be borrowed for two weeks.
For a personal retention copy, call
Tech. Info. Division, Ext. 6782.*



LBL-12122
e.2

DISCLAIMER

This document was prepared as an account of work sponsored by the United States Government. While this document is believed to contain correct information, neither the United States Government nor any agency thereof, nor the Regents of the University of California, nor any of their employees, makes any warranty, express or implied, or assumes any legal responsibility for the accuracy, completeness, or usefulness of any information, apparatus, product, or process disclosed, or represents that its use would not infringe privately owned rights. Reference herein to any specific commercial product, process, or service by its trade name, trademark, manufacturer, or otherwise, does not necessarily constitute or imply its endorsement, recommendation, or favoring by the United States Government or any agency thereof, or the Regents of the University of California. The views and opinions of authors expressed herein do not necessarily state or reflect those of the United States Government or any agency thereof or the Regents of the University of California.

CHARACTERIZATION OF LARGE DIAMETER SILICON BY
LOW-BIAS CHARGE COLLECTION ANALYSIS IN Si(Li) PIN DIODES

Abraham Fong¹, Jack T. Walton¹, Eugene E. Haller^{1,2},
Heinrich A. Sommer¹ and Jens Guldborg³

¹Lawrence Berkeley Laboratory
University of California
Berkeley, California 94720 U.S.A.

²Dept. of Materials Science and Mineral Engineering
University of California
Berkeley, California 94720 U.S.A.

³TOPSIL
3600 Frederikssund
Denmark

January 1981

This work was supported by the Assistant Secretary for Environment,
Office of Health and Environmental Research, Pollutant Characteriza-
tion and Safety Research Division of the U.S. Department of Energy
under Contract No. DE-AC03-76SF00098.

CHARACTERIZATION OF LARGE DIAMETER SILICON BY
LOW-BIAS CHARGE COLLECTION ANALYSIS IN Si(Li) PIN DIODES*

Abraham Fong^{1†}, Jack T. Walton¹, Eugene E. Haller^{1,2},
Heinrich A. Sommer¹ and Jens Guldberg³

¹Lawrence Berkeley Laboratory
University of California
Berkeley, California 94720 U.S.A.

²Dept. of Materials Science and Mineral Engineering
University of California
Berkeley, California 94720 U.S.A.

³TOPSIL
3600 Frederikssund
Denmark

ABSTRACT

Five silicon single crystals, ~ 5 cm in diameter, grown under different conditions were examined for their suitability as Si(Li) detector grade material. A correlation was found between a crystal growth process parameter and incomplete and nonhomogeneous charge collection in the finished Si(Li) detectors when biased at voltages much lower than normally applied in detector operation. Data are presented and a model based on the presence of interstitial defects is proposed to explain the observed results.

1. Introduction

Experiments involving the measurement of small fluences of particles (e.g. on space flights or in some heavy ion reactions) have prompted development of large diameter¹ silicon lithium drifted [Si(Li)] detectors (diameters 5 cm or greater). While large diameter silicon crystals are available, we have

*This work was supported by the Assistant Secretary for Environment, Office of Health and Environmental Research, Pollutant Characterization and Safety Research Division of the U.S. Department of Energy under Contract No. DE-AC03-76SF00098.

†Present address: National Semiconductor, 2900 Semiconductor Drive, Santa Clara, California 95051 U.S.A.

encountered some difficulties in obtaining complete charge collection efficiency throughout the lithium compensated volume of the detectors as their diameters have increased.

In an attempt to understand the causes of these difficulties, five 5 cm diameter silicon crystals with different, well controlled growth parameters were examined to determine the effects of growth conditions on the final Si(Li) detector charge collection characteristics.

2. Device Fabrication

2.1. Crystal Data

The study presented here was undertaken in collaboration with TOPSIL, Denmark, who supplied the silicon crystals. These are floating-zone, dislocation-free p-type crystals grown along the [111] axis. The five crystals were grown from three rods of polycrystalline silicon which were reduced from SiCl_4 . Two different processes were employed in zone refining: silicon for crystals 2 and 5 (poly-zoned rod 46-872) was zone refined exclusively in vacuum, whereas the silicon for crystals 1 (poly-zoned rod 1-340), 3 and 4 (poly-zoned rod 40-784) was zone refined in argon. The final single crystals were all grown in argon with two processes being employed: process I (crystals 1 and 2) and process II (crystals 3, 4 and 5). In process I the crystal is grown with a lower radiative heat loss than in process II, and process I operates with a larger melt flow pattern than process II. In addition to the two process parameters, two different crystal growing speeds were employed--high and low (high being 50% greater than the low). A summary of the crystal data and detectors fabricated is given in Table I.

Crystals which were pulled at a high speed (crystal 2, process I; crystals 4 and 5, process II) exhibited a crystal defect known as an etching depression²--i.e., where a wafer is exposed to a rapid etchant ($\text{HNO}_3:\text{HF}:3:1$), the central region will etch faster than the periphery. The diameters of the central depressions are listed in Table I. Preferential etching⁷ of the samples revealed the existence of swirl and striation patterns in the two crystals pulled at low speeds (crystal 1, process I light patterns; crystal 3, process II heavy patterns).

Profiles of the radial resistivity variations across the diameter of each crystal are given in Figure 1. As can be seen, there is very little radial resistance variation—less than $\pm 5\%$ in each of the five crystals.

2.2. Si(Li) PIN Diode Fabrication

Two types of experiments were conducted with these crystals. In the first, we fabricated Si(Li) devices for evaluation as radiation detectors while in the second, we determined the Li ion mobility at 110°C . In both of these, the following relationship between the lithium ion mobility μ and the depth of the lithium compensated region x is employed³:

$$x = (2\mu Vt)^{1/2} \quad (1)$$

where V is the applied voltage, which we normally measure in terms of kilovolts and t is the time, usually measured in terms of hours. The product Vt is then in kilovolt hours (kVhr).

The set of ten 3 mm thick Si(Li) detectors fabricated as listed in Table 2 are of the grooved type⁴ (Fig. 6). The lithium ion drift compensation was conducted at the relatively low temperature of 110°C and the moderate applied voltage of 500 volts to avoid high drift currents (i.e. to keep the reverse leakage currents on the devices during the lithium ion drift to less than 5 mA). The devices were subjected to a nominal 80 kVhr to ensure that the whole area and thickness of these devices was fully lithium compensated. The performance of these detectors is discussed in detail in Section 3.

To determine the Li ion mobility and the extent of any radial dependency, a set of 5 mm thick samples were lithium ion compensated at 110°C for 50 kVhr and then cut apart and copper stained¹⁷ to determine the depth of the Li ion compensation. The experimentally measured depths and the mobilities calculated using Equation 1 are listed in Table 2.

Table 2. Lithium Ion Mobility

Crystal	Measured Lithium Ion Depth	Calculated Lithium Ion Mobility
1	$2.91 \pm .04$ mm	2.3×10^{-10} cm ² /volt-sec
2	$3.02 \pm .04$	2.5×10^{-10}
3	$2.85 \pm .04$	2.3×10^{-10}
4	$2.80 \pm .04$	2.2×10^{-10}
5	$2.69 \pm .04$	2.0×10^{-10}

Pell⁵ has derived an equation for the diffusion coefficient, D, of lithium in silicon as:

$$D \text{ (cm}^2\text{/sec)} = 2.3 \times 10^{-3} \exp (-0.645 q/kT) \quad (2)$$

where $q = 1.6 \times 10^{-19}$ Coulombs, $k = 1.38 \times 10^{-23}$ Joules/K and in our case $T = 383$ K (110°C). This yields a value for the diffusion coefficient of 7.6×10^{-12} cm²/sec or a lithium ion mobility at 110°C of 2.3×10^{-10} cm²/volt-sec. The experimental results are in good agreement with the value obtained from Pell's equation. Further, no radial dependence of the lithium ion mobility was observed; the variations obtained are due to measurement errors and not due to any observed radial variation in the lithium ion drift depth.

3. Si(Li) Detector Experiments

3.1. Low Field Charge Collection Studies

Two 3 mm thick, 1500 mm² Si(Li) detectors were fabricated¹ from each of the five crystals. We normally scan across the Au-Schottky barrier (which will be called the p-contact in the following) of newly processed detectors with an ²⁴¹Am alpha source collimated to 2 mm to test for uniformity and charge collection efficiency (Figure 2). In normal detector operation, the detectors are reverse biased to provide a uniform field of ~ 1300 V/cm. For detectors made from crystal 3, there was evidence of nonuniform charge

collection became worse with decreasing electric fields. Consequently, the performance of the detectors fabricated from the five sample crystals was examined at fields ~10 to 100 times lower than those normally used.

At these low voltages (< 50 V), it might be suggested that the detectors may not be totally depleted due to non-ideal lithium compensation. Because lithium is drifted from the n contact to the p contact, it might be assumed that the region of poorest compensation lies in the vicinity of the p contact. Such a poorly compensated region would be undepleted at low reverse voltages, leading to a "window problem" which might account for a charge collection deficiency. We found that this is not the case, and show in the Appendix that p contact dead layers or windows are not a problem in our measurements.

3.2. Electron Collection - Alpha Particles Through the P Contact

For the test arrangement shown in Fig. 2 the charge collected when alpha particles enter the p contact is induced by electron traversal⁶. Figures 3A - 3E show the pulse height produced by the charge collected from an alpha scan of a detector from each of the five crystals for various applied voltages. There is a strong difference in the collection characteristics of these detectors. Detectors made from crystals 3, 4 and 5 show a characteristic dip in the signal height at low bias. Detectors made from crystals 1 and 2 show no dip, and in fact detector 3781 actually shows a slightly larger signal in the center at low bias. These characteristics hold for all four detectors made from crystals 1 and 2, and for all six detectors made from crystals 3, 4 and 5.

Comparing these findings with the crystal parameters in Table I shows the detector performance to be well correlated with the floating zone process— process I crystals (1 and 2) produced detectors which exhibited homogeneous and relatively high charge collection at low applied bias, while process II crystals (3, 4 and 5) produced detectors which exhibited nonhomogeneous and relatively low charge collection at low applied bias.

Detectors made using the process I crystals showed remarkable homogeneity. Figure 4a shows oscilloscope traces of pulses out of the preamplifier (Fig. 2) with a process I detector (3781) biased at 10 volts and the alpha source directed at four different locations on the p contact. Figure 4b shows a signal from the same detector with no applied bias and at -180°C .

In contrast with process I crystals, no alpha signals above the noise could be obtained for unbiased process II detectors. Detectors from crystal 3

even showed nonuniform charge collection at our normal operating voltage of 400 volts for a 3 mm thick detector.

As noted earlier, crystal 3 exhibited a heavy swirl and striation pattern. Figure 5b shows an alpha scan of detector 3786 biased at 150 v, made from crystal 3, along with a photograph (Fig. 5a) of the cross section of a companion sample which has been selectively etched (Secco etch⁷). The striking correlation between the regions with and without striations, and with and without signal degradation is evident. The lines connecting points in Fig. 5b indicate the presence of multiple peaks. Even at our normal operating voltage of 400 volts for 3 mm thick detectors, an annular region with a charge collection deficiency of about 1% for alphas entering the p contact was present on detectors made from this crystal. The defects which are responsible for the swirl patterns are evidently also associated with poor charge collection. We believe that a related defect is also responsible for the poor low voltage performance of detectors made from crystals 4 and 5. All four detectors 3791 - 3794 from crystals 4 and 5 exhibit incomplete charge collection in their central regions at low voltages.

3.3. Hole Collection - Alpha Particles Through the N Contact

Up to this point we have only discussed charge collection due to electrons. The detectors fabricated from the test crystals have a lithium layer as the n contact which is 120 - 150 μm thick (Figure 6a). Such a thick layer prevents the study of hole traversal in these detectors with natural alpha sources, since the alphas from these sources have a range of only $\sim 25 \mu\text{m}$ in silicon.

However, some detectors were available which were fabricated from a crystal grown under the same conditions as crystal 5. They are of the thin-window type¹ (Figure 6b)—having lithium n contact which is only $\sim 10 \mu\text{m}$ thick. This enabled us to observe hole traversal by scanning the alpha source across the n contact of these detectors. Since these detectors were already fabricated, we decided to employ them in our studies on hole collection rather than subjecting our test detectors to the additional processing required to obtain the thin lithium n contacts. This substitution is justified by the fact that the growth conditions for the crystal from which the thin-window detectors were made were similar to that for crystal 5 and the observation that the electron traversal is similar to that of the detectors made from crystals 3, 4 and 5.

The preamplifier signals due to electron traversal at two different positions (center and periphery) in one of these thin-window detectors (4182) with 35 volts bias are shown in Fig. 7. The waveforms show a characteristic linearly rising portion which indicates a uniform electric field near the p contact (see Appendix). However, electrons traversing at the detector center appear to be trapped midway across the detector. This same characteristic is found in the signal waveforms of our detectors made from crystals 3, 4 and 5. On the basis of similar signal waveforms and crystal growth conditions, we are confident that the alpha particle scanning results discussed in the next paragraph which were obtained with the thin n-contact detectors are also relevant for our detectors made from crystals 3, 4 and 5.

Scanning with the alpha source across the n contact of detector 4182 again biased at 35 volts yielded the results shown in Fig. 8a for hole traversal across the detector. Note that the initial slopes on the waveforms for the source at the detector center and periphery are again identical indicating that the electric field is also uniform at the n contact. It appears that the holes are also trapped about midway while traversing the detector central area as was observed previously for electron traversal. Figure 8b shows the waveform with 50 volts applied bias. At this bias the holes manage to traverse the full depth of the detector, but a slight irregularity can still be seen about midway through the rise of the waveform. This was also observed for electron traversal. In general, it was found that signals obtained from hole traversal behaved in much the same way as signals due to electron traversal.

3.4. Charge Collection Temperature Dependence

In order to gain further insight into the charge trapping mechanism, we studied the performance of the detectors in the temperature range -196°C to 22°C . Process II detectors were found to have increasingly poorer low voltage charge collection with decreasing temperatures. In contrast, process I detectors showed little variation in charge collection efficiency with temperature.

3.5. Cleanup Drift Effects

The low voltage charge collection properties of the process II crystals are improved somewhat after a cleanup drift⁸. Figure 9 shows the results of an alpha scan on detector 3785 (crystal 3) before and after a cleanup drift at

200 volts and 100°C for 16 hours. The improvement in the charge collection with 30 volts bias is evident. However the device performance is still considerably poorer than that of detectors made from process I crystals.

4. Discussion

Of the three parameters varied on our sample crystals, process I and II, pull speed high and low, and zone-refining ambient vacuum or argon, the dominant factor in the detector performance is the process parameter. The presence of swirls in crystal 3, which are well correlated with regions of incomplete charge collection, strongly suggests that the problems in charge collection with the process II crystals are linked to the formation of micro-defects in the crystals. The differences between the I and II processes are the following:

- a) process I has a lower radiative heat loss than process II,
- b) process I operates with a larger volume of molten silicon than process II, and
- c) the downward flow of molten silicon in process I is distributed over a larger cross section than process II.

To explain how these differences could affect the generation of micro-defects in our silicon crystals, it is necessary to refer to some of the models that have been proposed for microdefect formation in float-zoned silicon crystals. Theories presented by Chikawa and co-workers^{9,10} and by Föll et al¹¹ postulate that swirl defects are complexes formed through interaction between interstitial silicon atoms and residual impurities having low segregation coefficients, most likely carbon. Nuclei formation is believed to be controlled to a large extent by fluctuations in the growth rate accompanied by impurity striations, whereas the size of the defect is governed by the cooling rate of the crystal. For example, it has been demonstrated that lowering the cooling rates in the extreme will cause the dissolution of swirl defects¹². However, the cooling rate for process I crystals is not in this low region where dissolution takes place. Consequently, the difference in defect formation between the two processes is likely due to the volume of molten silicon involved.

Defect structures in the silicon crystal may vary from complicated dislocation loops (A swirls), at times decorated with impurity precipitates, to small agglomerates (B swirls) with strain fields small enough to go undetected

by TEM analysis. The A swirl defects are believed to evolve from the B swirl defects¹³. In the previously noted model of Chickawa and also in the analysis of Mühlbauer and Sirtl¹⁴, the microscopic nonuniform temperature of the crystals at the solidification interface is proposed as a possible cause for the generation of swirl defects.

The process I operates with a larger volume of molten silicon and the downward flow in the center is distributed over a larger cross section of the melt than with process II, both of which work to stabilize the isotherms around the solidification interface and thereby reduce the B swirl generation. Consequently for the process I crystals with the pull speeds used in our experiments, defects apparently are not generated. However for process II crystals, the defects are generated, possibly along with embryonic defect complexes similar to B swirls. The A swirl defects are readily apparent in crystal 3 (Fig. 5b), and while these defects were eliminated in crystals 4 and 5 by increasing the pulling speed, the centers of the detectors made from these crystals were still acting as regions with incomplete charge collection at low voltages indicating the presence of defects.

Our lithium ion mobility results on these crystals, with measured values within 13% of the expected value, disagree with the work of Guislain et al¹⁵. They reported lithium ion mobilities 15 to 90% below the expected value and attributed this to the presence of point defects caused by vacancy clusters. (Recent developments indicate that the defects are due to silicon interstitials rather than vacancies¹³). We surmise from Guislain's data that they had crystal growth conditions which produced a high density of B-type defects, which in some cases coalesced into clusters (A swirls). In the crystals for which clustering occurred, the lithium ion mobility was near the expected value, whereas in those which were free of A swirls the lithium mobility was low. This leads to the conclusion that if pre-B or B-type defects are present in sufficient density and are distributed throughout the crystal, then the lithium ion mobility can be affected by their presence. Since our measured lithium ion mobilities are close to the expected value, the B-type defect density in our crystals must be sufficiently low as to not adversely affect the lithium ion drift. The defect density in the process II crystals, however, is apparently sufficient to produce effects on electrons and holes moving through the detectors made from these crystals.

A quantitative treatment of our charge collection data based on the effects of interstitial microdefects is difficult due to the variety of signal charge versus time dependencies encountered. However, it is possible to qualitatively explain our observations. For crystal process II detectors with low bias, many of the electric field lines are affected by the interstitial defects which will cause the charge carriers to pass near the defect and be trapped with a small binding energy. As the bias is increased, more field lines traverse the detector uninterrupted and the charges are swept by the interstitials without being trapped. A clean-up drift seems to have the effect of decreasing the trapping cross section (perhaps by the lithium ion associating with the defect) and thereby improving the charge collection efficiency. That this improvement does not persist with time can be explained by the lithium precipitating at the defects¹⁵. The increased charge trapping at low temperatures can be attributed to the reduction in thermal energy available to detrapp the signal charges from the defects.

Examination of our devices with Deep Level Transient Spectroscopy¹⁶ (DLTS) indicates that these interstitial complexes do not represent single level traps in the bandgap of Si. No sharp DLTS peaks were observed in any of our detectors, which further supports our model in which the charge collection deficiency is due to extended structures.

5. Conclusion

A charge collection deficiency in finished Si(Li) detectors has been identified as being related to the formation of defects during crystal growth. The presence of defects appears to be related to the melt cross section. Detectors made from crystals grown with a large melt cross section (process I) exhibit uniform charge collection at low biases, whereas those grown with smaller cross sections (process II) demonstrate nonuniform or incomplete charge collection. We have proposed that impaired detector performance occurs in regions where fluctuations in the melt patterns perturb the nucleation process and produce defect complexes similar to the early stages of swirl generation. By characterizing these defect structures as trapping centers, we can qualitatively account for our experimental observations.

In all of our crystals, the lithium ion mobility is in good agreement with the expected value. With the exception of crystal 3 all had, at normal operating voltages ($V \approx 400$ V), good charge collection characteristics over their entire volumes. However, the results on crystal 3 and the related performance of the other process II crystals at low bias voltages indicate that if the crystal-growth-induced microdefects (pre B or B swirls) are sufficiently prevalent, the detector charge collection properties are deleteriously affected. Further, at even higher microdefect densities, the lithium ion mobility can apparently be degraded.

As indicated in our characterization of the five sample crystals, the technique of examining the Si(Li) detector charge collection performance with low bias voltages is very sensitive to the presence of microdefects in the crystal. The technique is useful in assessing the suitability of silicon crystals for large area detector fabrication and may also prove to be useful in relating crystal growth conditions to the crystal defects.

6. Acknowledgements

We appreciate the discussions with and interest of F. S. Goulding during the course of this work and the comments of R.H. Pehl in reviewing the manuscript.

7. Appendix

In operating detectors at the low voltages which we have employed in our tests, it could be argued that the observed results are not related to the detector bulk properties, but rather due to the entrance window properties. Variations in these windows could occur due to incomplete lithium compensation near the p contact or incomplete lithium compensation in the bulk leading to a very low electric field or variations in this field at the p contact. The first argument can be answered by the fact that each detector was copper stained¹⁷ to detect the presence of lithium at the p contact. For each detector, lithium decoration was observed over the full detector area. The second argument requires two facts to dismiss. First, the capacitance-voltage depletion characteristic for each device was measured and full depletion was found

to occur between 5 to 15 volts (some devices required a cleanup drift to achieve this). The electric field lines are therefore reaching the p contact at these voltages. Second, variations in the electric field strength can be estimated from the transient response of the charge signal. For charge signals introduced near the p contact in a detector having trapping centers with long detrapping times, the expected signal as a function of time, t , has the form⁶:

$$Q(t) = \frac{Q_0 \tau^+ \mu E}{L} (1 - \exp^{-t/\tau^+}) \quad t < T_R \quad (3)$$

where Q is the incident charge (generated in our case by the alpha particles), τ^+ is the mean time a carrier is free before being trapped, μ is the carrier mobility, E the electric field strength, and T_R the time for the carriers to traverse a trap-free detector of thickness L . Now:

$$\left. \frac{dQ(t)}{dt} \right|_{t=0} = \frac{Q_0 \mu E}{L} \quad (4)$$

so that any variations in the field strength, E , appear as changes in the slope of the initially rising charge signal. In all of our detectors no variations in the initial slope in the charge signal, $Q(t)$, between regions of poor and good charge collections efficiency at low voltages were observed. Consequently, from these arguments it can be concluded that variations in the charge collection at the p contact window regions are not a problem in our measurements, and that the variations in charge collection observed in scanning across the detectors are due to a detector bulk material problem.

References

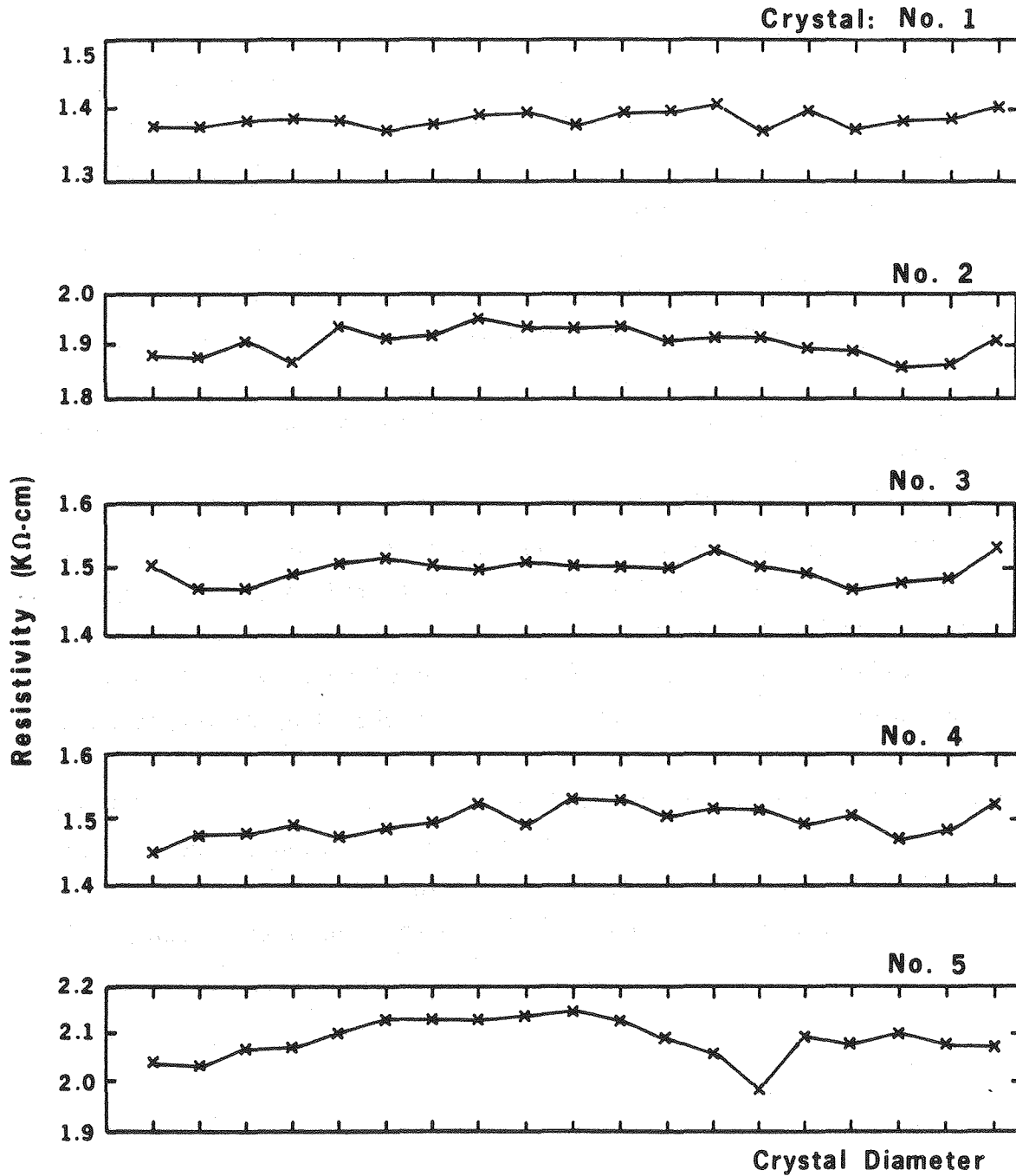
- [1] J.T. Walton, H.A. Sommer and D.E. Greiner, I.E.E.E. Trans. Nucl. Sci. NS-25 (1) (1978) 391.
- [2] W. Keller and A. Mühlbauer, Inst. Phys. Conf. Ser. 23 (1975) 538.
- [3] E.M. Pell, J. App. Phys. 31, No. 2 (1960) 291.
- [4] J. Llacer, IEEE Trans. Nucl. Sci. NS-11 (3) (1964) 221.
- [5] E.M. Pell, Physical Review Vol. 119, No. 4 (1960) 1222..
- [6] J.W. Mayer, Semiconductor Detectors (eds. G. Bertolini and A. Coche; North-Holland Publ. Co., Amsterdam 1968) Ch. 5.
- [7] F. Secco d'Aragona, J. Electrochem. Soc. 119 (1972) 948.
- [8] A. Lauber, Nucl. Instr. and Meth. 75 (1969) 297.
- [9] J. Chikawa and S. Yoshikawa, Solid State Technology 23 (1) (1980) 65.
- [10] J. Chikawa and S. Shirai, J. Crystal Growth 39 (1977) 328.
- [11] H. Föll, U. Gösele and B.O. Kolbesen, J. Crystal Growth 40 (1977) 90.
- [12] P.S. Roksnoer, W.J. Bartels and C.W.T. Buhle, J. Crystal Growth 35 (1976) 245.
- [13] A. Seeger, H. Föll and W. Frank, Inst. Phys. Conf. Ser. 31 (1977) 12.
- [14] A. Mühlbauer and E. Sirtl, Phys. Stat. Solidi (a) 23 (1974) 555.
- [15] H.J. Guislain, W.K. Schoenmaekers and L.H. Delaet, Nucl. Inst. and Meth. 101 (1972) 1.
- [16] E.E. Haller, P.P. Li, G.S. Hubbard and W.L. Hansen, I.E.E.E. Trans. Nucl. Sci. NS-26, 1 (1979) 265.
- [17] P.A. Iles and P.J. Coppen, J. Appl. Phys. 29 (1958) 1514.

Table I. Crystal Data.

<u>Crystal No.</u>	<u>Detector</u>	<u>Zone Refined Polynumber</u>	<u>Poly-Prod. Atmosphere</u>	<u>O-EPD Speed</u>	<u>Float-Zone Process</u>	<u>Diameter of Etch Depression (mm)</u>	<u>Swirl Pattern</u>
1	3781, 3782	1-340	Argon	Low	I	0	Light
2	3783, 3784	46-872	Vacuum	High	I	25	None
3	3785, 3786	40-784	Argon	Low	II	0	Heavy
4	3791, 3792	40-784	Argon	High	II	30	None
5	3793, 3794	46-872	Vacuum	High	II	38	None

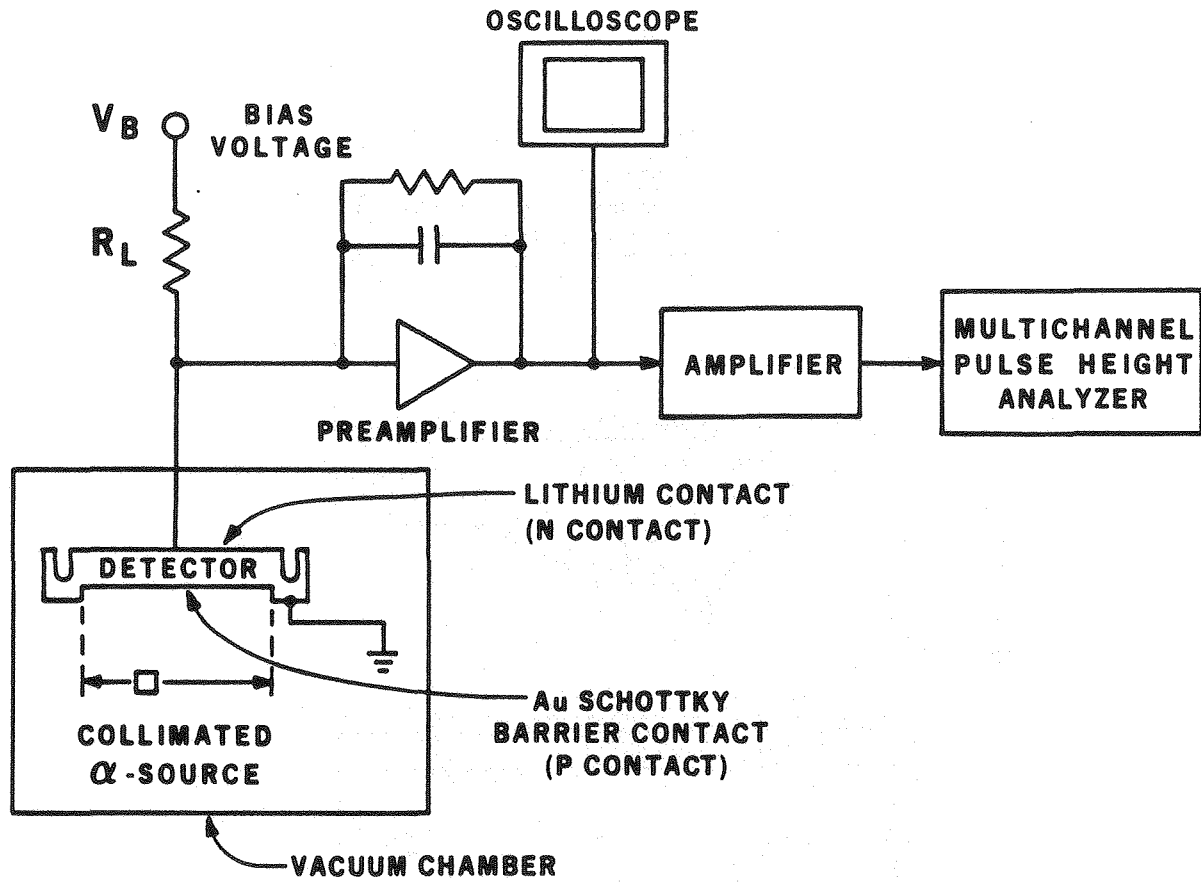
Figure Captions

1. Radial resistivity profiles of each of the five sample crystals.
2. Test setup for α -scan.
3. The α -scans of detectors from each of the five sample crystals 1 - 5 (a - e) at various applied voltages. The lines connecting the points in (c) and (d) indicate the presence of multiple peaks. The vertical axis in each case is uncalibrated.
- 4a. The α -scan of detector 3782 at 10 volts bias. Radial positions are -15, -5, +5, +15 mm with respect to the center (50 mV and 2 μ s/div.).
- 4b. A typical process I crystal detector waveform with no applied bias at -180°C (10 mV and 20 μ s/div.).
- 5a. A Secco etch of a longitudinal section of a crystal number 3 illustrating a striation pattern.
- 5b. An α -scan of detector 3786 at 150 volts bias.
6. (a) normal and (b) thin-window Si(Li) detectors. Shown are the cross-sections of the devices with the Si(Li) compensated regions, the Li n contact, and the p contact.
7. Charge waveforms from detector 4182 biased at 35 volts with the α -particles impinging on a center point and on a peripheral point (20 mV and 1 μ s/div.).
8. The waveforms are at the center and periphery under the same conditions as in Fig. 7, except that the α -particles are impinging on the n contact, illustrating hole traversal (20 mV and 2 μ s/div.).
9. An α -scan of a process II detector (3785) before and after cleanup drift.



XBL 813-8338

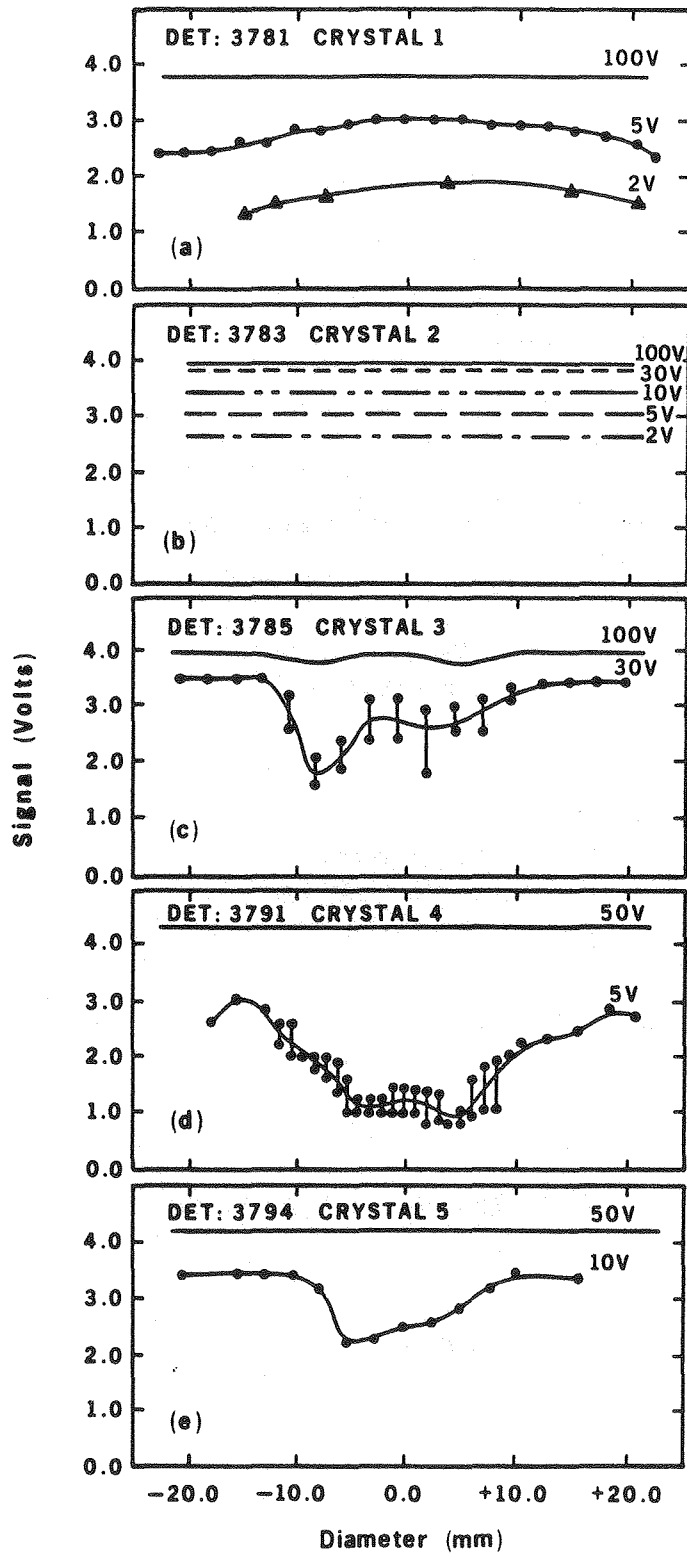
Fig. 1. Radial resistivity profiles of each of the five sample crystals.



TEST SETUP FOR α -SCAN

XBL 813-3887A

Fig. 2. Test setup for α -scan.



XBL 813-8332A

Fig. 3. The α -scans of detectors from each of the five sample crystals 1 - 5 (a - e) at various applied voltages. The lines connecting the points in (c) and (d) indicate the presence of multiple peaks. The vertical axis in each case is uncalibrated.

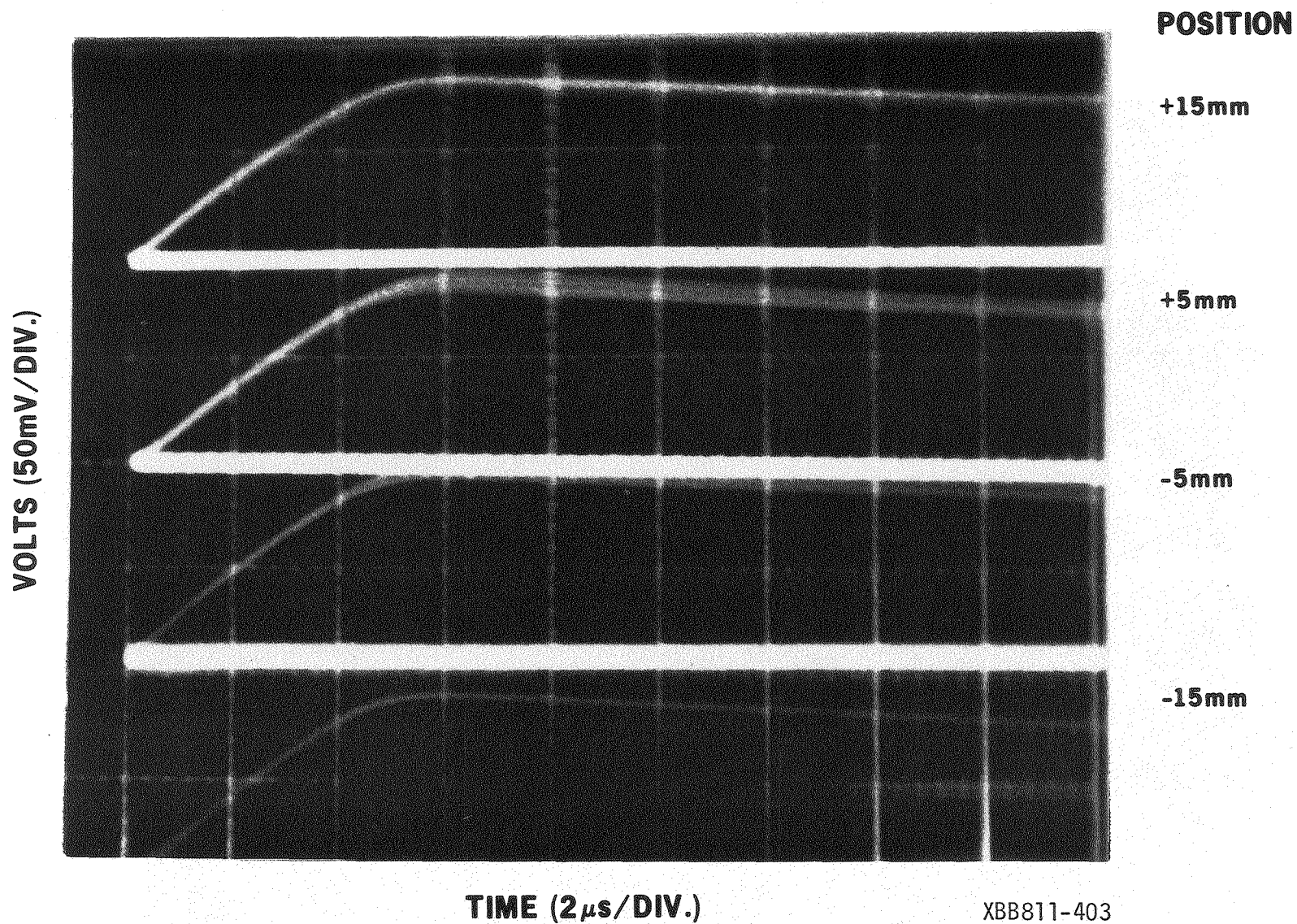
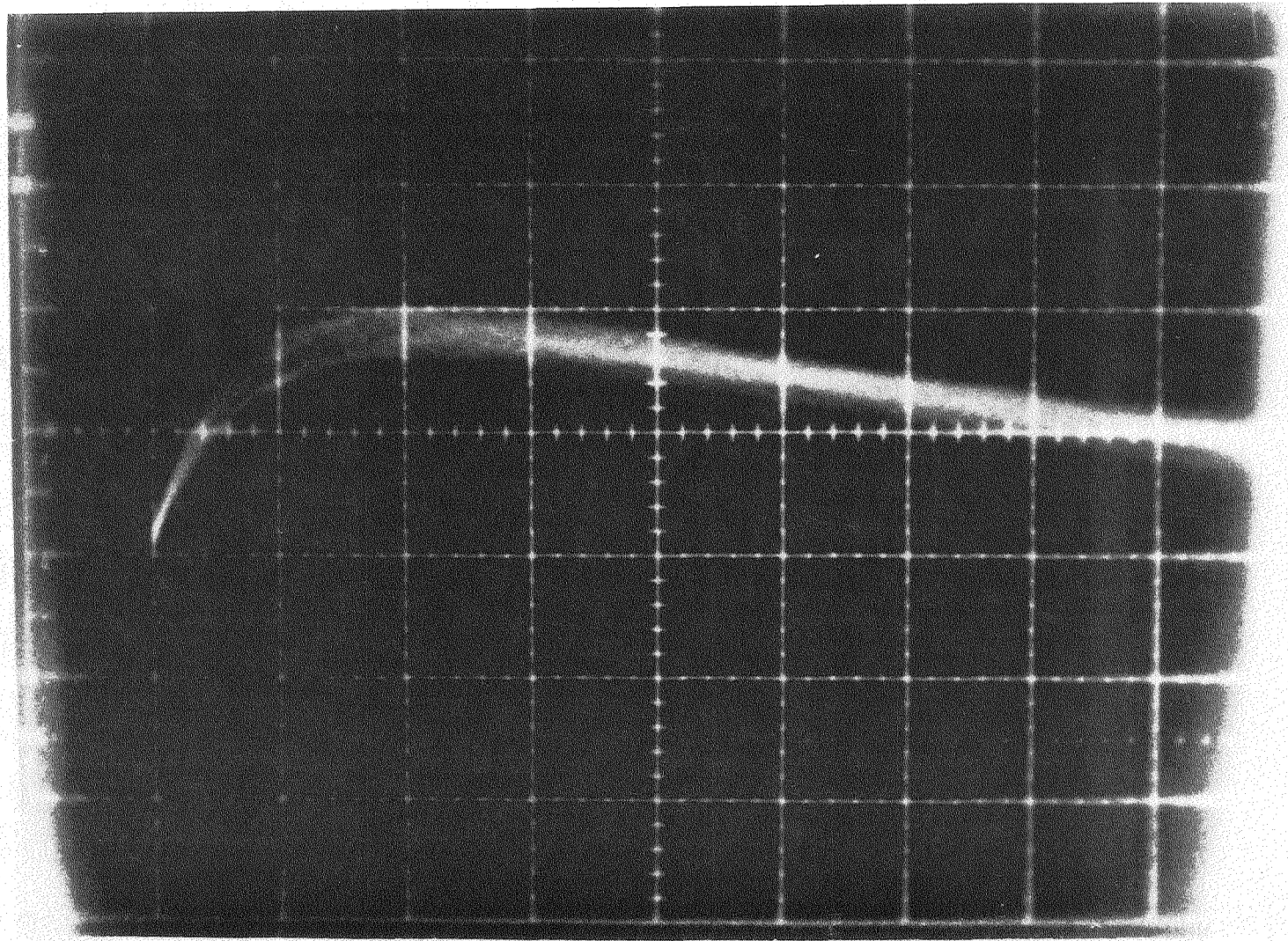


Fig. 4a. The α -scan of detector 3782 at 10 volts bias. Radial positions are -15, -5, +5, +15 mm with respect to the center (50 mV and 2 μ s/div.).

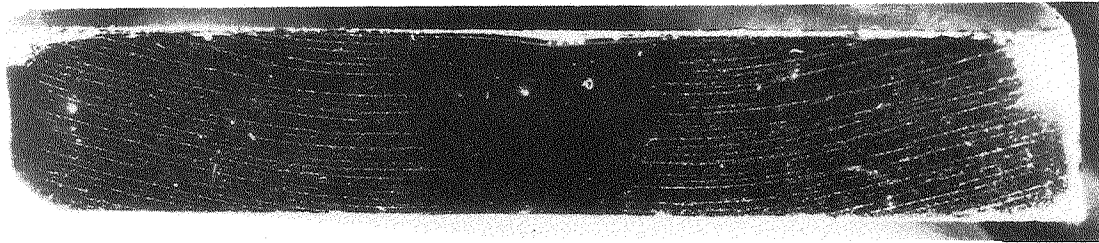
VOLTS (10mV/DIV.)



XBB811-405

TIME (20 μs/DIV.)

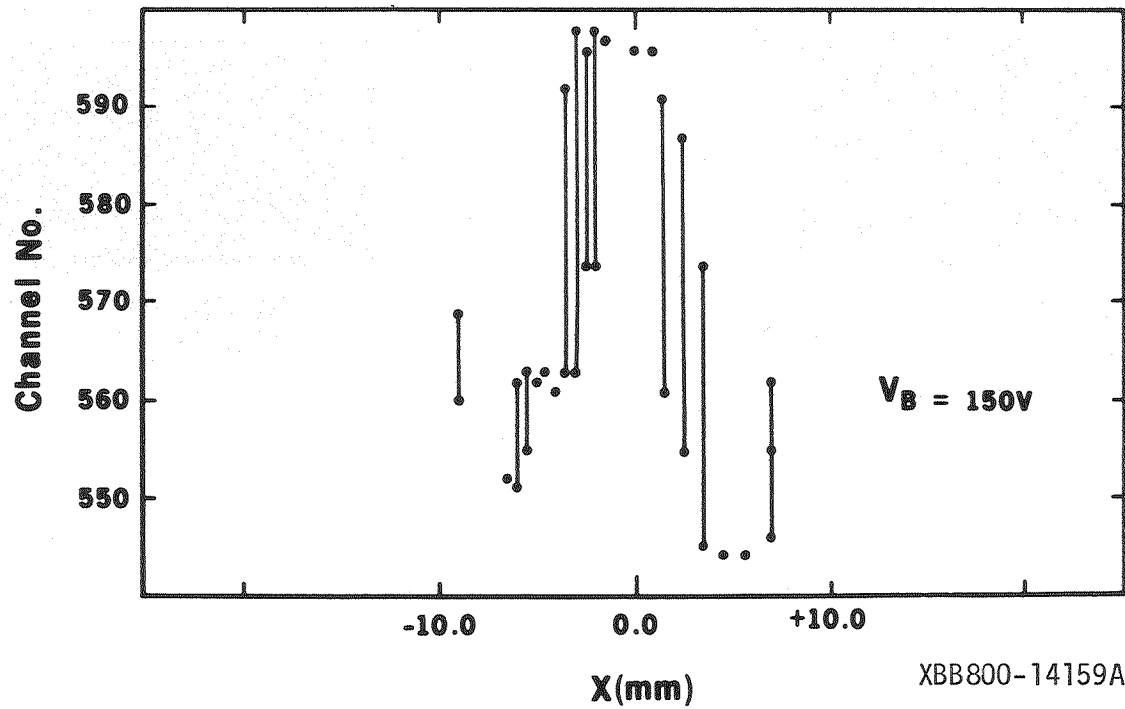
Fig. 4b. A typical process I crystal detector waveform with no applied bias at -180°C (10 mV and 20 $\mu\text{s}/\text{div.}$).



(5A)

Fig. 5a. A Secco etch of a longitudinal section of a crystal number 3 illustrating a striation pattern.

α -scan #3786 Xtal 3



(5B)

Fig. 5b. An α -scan of detector 3786 at 150 volts bias.

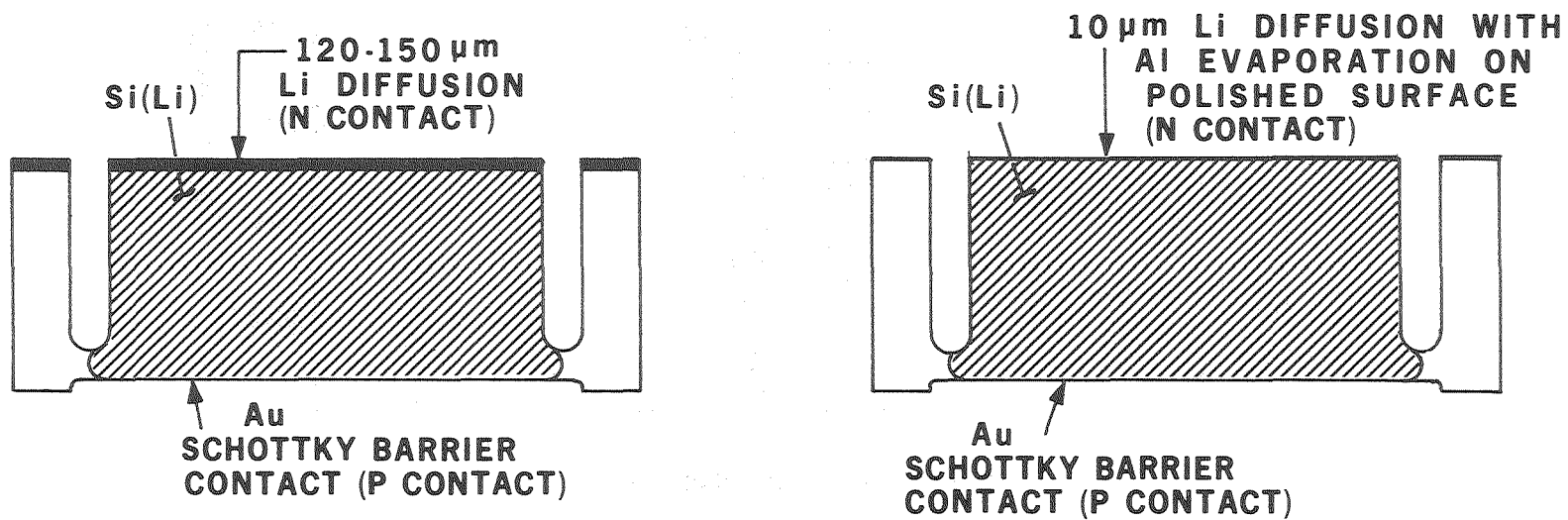


Fig. 6. (a) normal and (b) thin-window Si(Li) detectors. Shown are the cross sections of the devices with the Si(Li) compensated regions, the Li n contact, and the p contact.

XBL 7710-10098

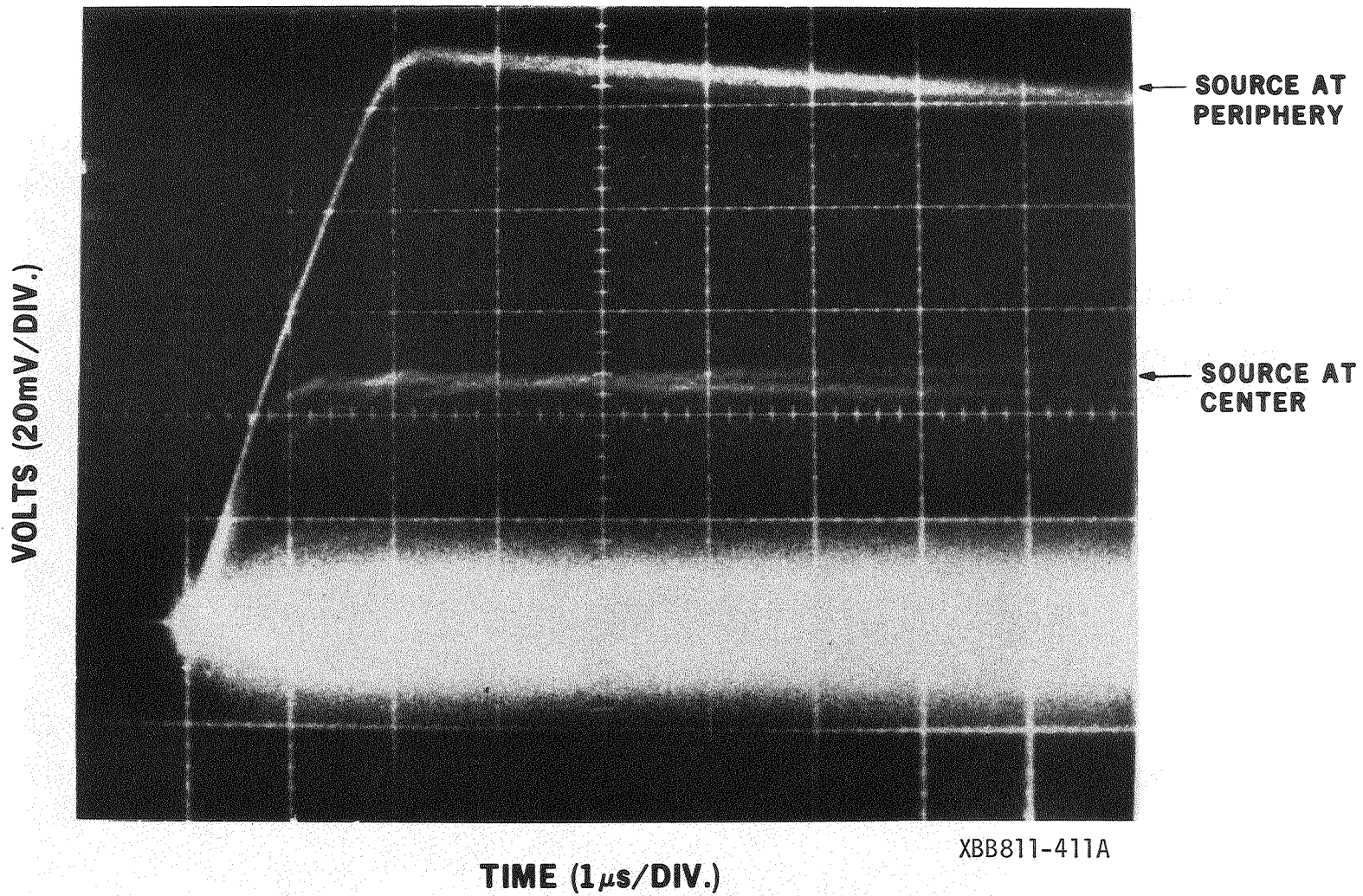


Fig. 7. Charge waveforms from detector 4182 biased at 35 volts with the α -particles impinging on a center point and on a peripheral point (20 mV and 1 μ s/div.).

(a) VOLTS (20mV/DIV.) (b)

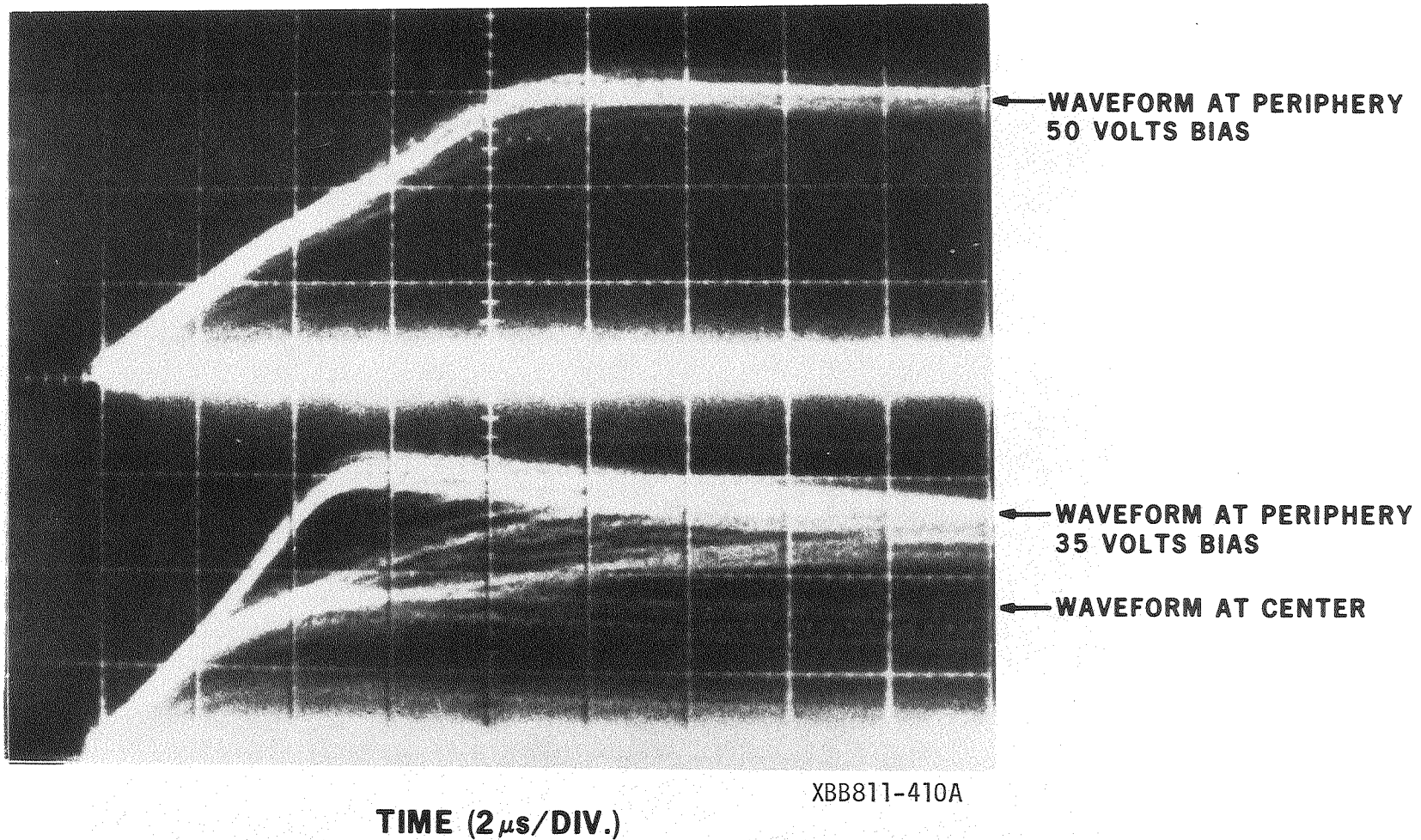
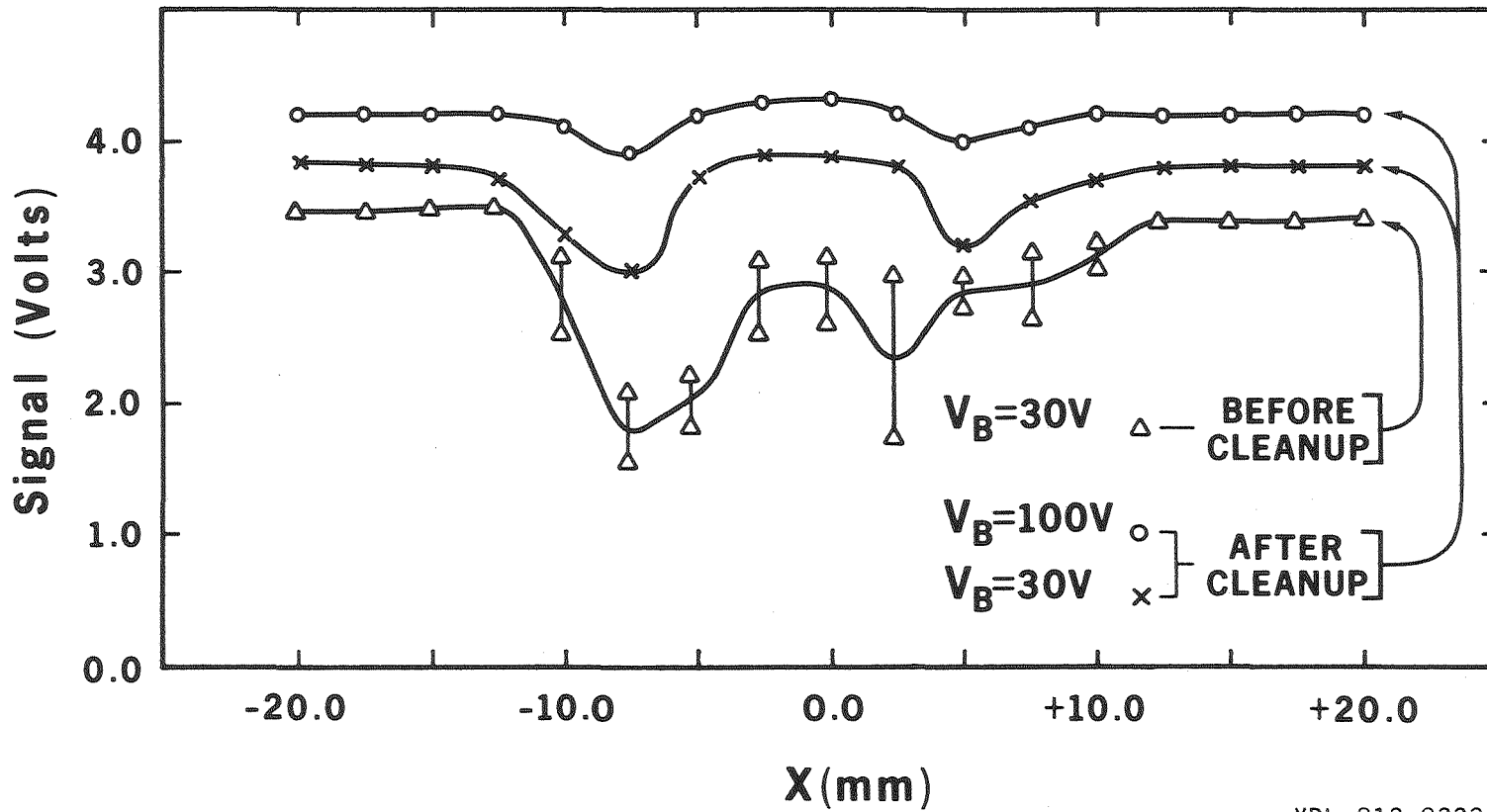


Fig. 8. The waveforms are at the center and periphery under the same conditions as in Fig. 7 except that the α -particles are impinging on the n contact, illustrating hole traversal (20 mV and 2 $\mu\text{s}/\text{div.}$).

Crystal 3B #3785



XBL 813-8333A

Fig. 9. An α -scan of a process II detector (3785) before and after cleanup drift.

